Bioactive Materials 24 (2023) 174–184

Contents lists available at ScienceDirect

Bioactive Materials

journal homepage: www.keaipublishing.com/en/journals/bioactive-materials

Engineering of immunoinstructive extracellular matrices for enhanced osteoinductivity

Andrés García-García [a,*], Sébastien Pigeot [a,b], Ivan Martin [a,b,**]

[a] Department of Biomedicine, University Hospital Basel, University of Basel, 4031, Basel, Switzerland
[b] Department of Biomedical Engineering, University of Basel, 4123, Allschwill, Switzerland

ARTICLE INFO

Keywords:
Immunomodulation
Bone tissue engineering
Inflammation
Hypertrophic cartilage matrices
Osteoinduction

ABSTRACT

The increasing recognition of the contribution of the immune system to activate and prime regeneration implies that tissue engineering strategies and biomaterials design should target regulation of early immunological processes. We previously proposed the cell-based engineering and devitalization of extracellular matrices (ECMs) as a strategy to generate implant materials delivering custom-defined signals. Here, in the context of bone regeneration, we aimed at enhancing the osteoinductivity of such ECMs by enriching their immunomodulatory factors repertoire. Priming with IL1β a cell line overexpressing BMP-2 enabled engineering of ECMs preserving osteoinductive signals and containing larger amounts of angiogenic (VEGF) and pro-inflammatory molecules (IL6, IL8 and MCP1). Upon implantation, these IL1β-induced materials enhanced processes typical of the inflammatory phase (e.g., vascular invasion, osteoclast recruitment and differentiation), leading to 'regenerative' events (e.g., M2 macrophage polarization) and ultimately resulting in faster and more efficient bone formation. These results bear relevance towards the manufacturing of potent off-the-shelf osteoinductive materials and outline the broader paradigm of engineering immunoinstructive implants to enhance tissue regeneration.

1. Introduction

Long lasting research in osteoimmunology has revealed the important cross-talk between bone and immune cells to finely regulate bone homeostasis and regeneration [1,2]. After bone fracture, new bone is typically formed recapitulating the embryonic developmental process of endochondral ossification, in which recruited mesenchymal stromal cells (MSCs) differentiate into chondrocytes to form a transient hypertrophic cartilage (HyC) callus. This tissue serves as a template for vascular cells, osteoprogenitors and hematopoietic progenitors to operate a gradual remodeling into bone and bone marrow (BM) [3]. In contrast to embryonic endochondral ossification, bone fracture healing is tightly coupled to an immune reaction that modulates the regenerative process. Immediately after the injury, innate immune cells – including monocytes, granulocytes, and macrophages - infiltrate into the hematoma and release cytokines inducing acute inflammation. After this inflammatory phase, immunomodulating MSCs and immune cells such as alternatively activated M2 macrophages orchestrate a process that resolves inflammation and favors tissue regeneration [4–7].

In the context of bone regeneration, multiple immunomodulatory strategies have emerged to generate cell-based biomaterials that can elicit a favorable innate immune reaction upon *in vivo* implantation and thus promote bone healing [8]. In contrast to chronic inflammation, inflammation was reported essential for bone regeneration if timely resolved [9–11], and the effect of several inflammatory factors (e.g., Tumor Necrosis Factor alpha (TNFα), Interleukin 1 beta (IL1β), Interleukin 6 (IL6), Interleukin 8 (IL8) and Monocyte Chemoattractant Protein 1 (MCP1)) on immune cells during this early phase was shown to lead to enhanced osteogenesis and angiogenesis [12–18]. Despite this generated knowledge, most immunomodulatory strategies targeting regenerative processes aim at the resolution of the inflammatory phase by inducing anti-inflammatory/immunosuppressive signals [19], while the correct activation of the acute inflammatory phase remains underexplored.

We previously engineered a human mesenchymal cell line overexpressing Bone Morphogenetic Protein 2 (BMP-2) (MSOD-B) capable of robustly generating *in vitro* human HyC. Even after devitalization, the resulting extracellular matrix (ECM) contained and delivered

Peer review under responsibility of KeAi Communications Co., Ltd.
* Corresponding author. Department of Biomedicine, University Hospital Basel, University of Basel, 4031, Basel, Switzerland
** Corresponding author. Department of Biomedicine, University Hospital Basel, University of Basel, 4031, Basel, Switzerland
E-mail addresses: andres.garcia-garcia@unibas.ch (A. García-García), ivan.martin@unibas.ch (I. Martin).

https://doi.org/10.1016/j.bioactmat.2022.12.017
Received 3 October 2022; Received in revised form 2 December 2022; Accepted 18 December 2022

osteoinductive signals, leading to efficient bone formation *in vivo* [20]. Here, we hypothesized that enriching the HyC in immunomodulatory signals targeting the early inflammatory phase that precedes tissue remodeling into bone during endochondral ossification would result in increased osteoinductivity. IL1β is a potent inflammatory factor that plays an important role in physiological bone metabolism by promoting osteoclastogenesis [21], but also during fracture repair by promoting osteoblasts proliferation and differentiation [13]. Here we identified IL1β as single inducer to prime human MSCs towards a pro-inflammatory profile during the chondrogenic differentiation phase, thereby engineering a HyC enriched in inflammatory/angiogenic signals cues as IL6, IL8, MCP1 and Vascular Endothelial Growth Factor (VEGF). The osteoinductivity of the resulting ECM-based material was assessed in a stringent ectopic model to measure *de novo* formation of bone tissue, decoupled from the process of osteoconduction from pre-existing bone structures. We found that materials generated by induction with IL1β were able to stimulate *in vivo* vascular invasion, M2 macrophage polarization and Receptor Activator for Nuclear factor Kappa beta Ligand (RANKL)-dependent osteoclast differentiation, resulting in accelerated remodeling and endochondral bone formation.

2. Material and methods

2.1. Cell culture

MSOD-B cells [20] were expanded in complete α-Minimum Essential Medium (αMEM) (CM) supplemented with 10% fetal bovine serum (FBS), 1% HEPES, 1% sodium pyruvate and 1% of penicillin–streptomycin–glutamine (PSG) solution (all from Gibco) and 5 ng/mL fibroblast growth factor-2 (FGF-2, R&D Systems) in a humidified incubator at 37 °C and 5% CO_2. RFP $^+$ Human Umbilical Vein Endothelial cells (HUVECs) were purchased from Angio-Proteomie (cat# cAP-0001RFP) and expanded in 2D monolayers in Endothelial Growth Medium 2 (EGM-2) (Lonza; cat# CC-3162). At 90% confluency, cells were detached using Trypsin-EDTA 0.05% (Gibco), counted and seeded again at a density of 6000 cells per cm^2.

2.2. In vitro drug acute treatments

MSOD-B cells were seeded in 12-well plates at a density of $1.3*10^4$ cells per cm^2 with supplemented CM and allowed to attach for 24 h. Then, the old medium was replaced by fresh medium supplemented with PBS, IL1β (0.1 ng/mL), TNFα (1 ng/mL), LPS (10 ng/mL), IL4 (10 ng/mL), Poly (i:c) 1 μg/mL or TGFβ1 (10 ng/mL) and cultured for another 24 h. After this time, supernatants were collected and stored at −20 °C, while cells were lysed with Lysis Buffer (Quick-RNA™ Mini Prep Kit; Zymo Research) for further RNA extraction.

2.3. Generation of in vitro immunomodulatory 3D HyC ECMs

HyC tissues were generated as previously described [20]. MSOD-B cells were seeded at a density of $2*10^6$ cells in 35 μL on top of 6 mm-diameter collagen type I cylindric sponges (Avitene Ultrafoam, BD). These collagen scaffolds were previously placed in 12-well cell culture plates coated with 2% agarose to prevent cell adhesion to the plastic. Cells were first cultured for 1 h at 37 °C to facilitate their distribution within the scaffold and adherence to it. After this time, constructs (collagen scaffolds seeded with MSOD-B cells) were cultured in chondrogenic medium for 3 weeks to induce HyC tissue formation. The chondrogenic medium was composed of Dulbecco's Modified Eagle's Medium (DMEM) supplemented with PSG (Gibco), HEPES (Gibco), Sodium-Pyruvate (Gibco), Insulin-Transferrin-Selenium (ITS) (Gibco), Human Serum albumin (HSA) 0.12% (CSL Behring), 0.1 mM Ascorbic Acid (Sigma; cat#A5960), 10^{-7} M Dexamethasone (Sigma; cat# D4902) and 10 ng/mL Transforming Growth Factor Beta 3 (TGFβ3) (kindly provided by Novartis). Medium was replaced twice a week.

To generate immunomodulatory HyC tissues, IL1β (0.1 ng/mL) was added to the medium during the last week of chondrogenic differentiation (week 3), while vehicle solution was used as control.

2.4. Tissue devitalization

Mature control or immunomodulatory HyC tissues were cultured overnight in DMEM supplemented with AP20187 (B/B Homodimerizer; 10^{-7} M) (ApexBio; cat# B1274) to induce cell apoptosis. Samples were then washed with PBS and processed for further analyses. The efficacy of this devitalization method was previously validated [22].

2.5. RNA isolation, reverse transcription and quantitative real-time PCR (RT-qPCR)

Total RNA extraction was performed using Quick-RNA™ MiniPrep Kit (Zymo Research; cat# R1055), which includes treatment with DNAse I (Invitrogen) to eliminate contaminating genomic DNA. Reverse transcription into cDNA was performed using SuperScript III Reverse Transcriptase (Invitrogen; cat# 18080–044), following the manufacturer's recommendations. Quantitative RT-qPCR assays were performed with ABIPrism 77000 Sequence Detection System (PerkinElmer/Applied Biosystem) and using TaqMan Universal PCR Master Mix (Applied Biosystems; cat# 4304437). Gene expression was estimated using 2ΔΔCT method and normalized to housekeeping *GAPDH* gene expression. TaqMan™ Gene Expression Assay mixes (Applied Biosystem; cat# 4453320) were used to measure the relative expression of the following genes: *IL6*, *IL8*, *MCP1*, *IL1β*, *VEGF*, *BMP2*, Collagen type II alpha 1 (*COL2A1*), Collagen type X alpha 1 (*COL10A1*), Matrix Metallopeptidase 13 (*MMP13*), *TNFα*, Interleukin 10 (*IL10*), Matrix Metallopeptidase 9 (*MMP9*) and Cathepsin K (*CTSK*).

2.6. Luminex assay

Protein content was determined using Human Magnetic Luminex Assay (R&D Systems; cat# LXSAHM) according to manufacturer's instructions. The following analytes were measured: IL6, IL8, MCP1 and VEGF. The concentration of these factors was normalized to the total amount of protein in the engineered tissue to exclude any effect that IL1β induction could have to the cellularity of the tissue. To calculate these values, the concentration (ng/mL) obtained for each factor in the Luminex assay was then divided by the total protein concentration of the tissue (μg/mL). Total protein concentrations were calculated using PierceTM BCA Protein Assay Kit (ThermoFisher Scientific; cat# 23225), according to the manufacturer's instructions.

2.7. ELISAs

BMP2 protein quantification was assessed using the human BMP2 DuoSet ELISA (R&D Systems; cat# DY007B) according to the manufacturer's instructions. BMP2 concentration was then normalized to the total amount of protein as indicated above. Tartrate-resistant acid phosphatase (TRAP) quantification was performed using the human TRACP/PAP/ACP5 ELISA Kit (ThermoFisher Scientific; cat# EH461RB) following manufacturer's instructions.

2.8. Histological analysis

Engineered tissues were fixed by incubation in 2% paraformaldehyde (PFA) (vol/vol) for 24 h and, in case of mineralized tissues, decalcified in 15% Ethylenediamine tetraacetic acid (EDTA) solution (Sigma-Aldrich). Samples were cryoprotected with successive incubations in sucrose (15% sucrose for 4 h followed by 30% sucrose overnight). After a quick rinse in PBS samples were embedded in OCT (CellPath; cat# KMA-0100-00A). 10 μm-cryosections were obtained using a Leica Biosystems Cryostat (Leica). Safranin-O, hematoxylin &

eosin, TRAP and Trichrome de Masson (RAL Diagnostics) stainings were performed as previously described [16], and following manufacturer's instructions. Immunohistochemistry stainings for Collagen type II, Collagen type X, MMP13 and Osterix were performed following a regular protocol for cryosections in a humidified chamber. Briefly, tissues were blocked in 5% goat serum in Tris-Buffered Saline (TBS) for 10 min at room temperature. After a 5 min wash in TBS, samples were incubated with primary antibodies diluted in 1% Bovine Serum Albumin (BSA) in TBS overnight at 4 °C. The following primary antibodies were used: mouse anti-human Collagen II (MP Biomedicals; cat# 63171; 1/1000), mouse anti-human Collagen X (ThermoFisher; cat#14-9771-82; 1/100), rabbit anti-human MMP13 (Abcam; cat# ab39012r; 1/75), rabbit anti-mouse/rat Osterix (Abcam; cat# ab22552; 1/200), rat anti-mouse CD31 (Biotechne; cat# 553370; 1/200), rat anti-mouse F4/80 (Abcam; cat# ab6640; 1:200) and rat anti-mouse CD206 (Bio-Rad; MCA2235). After a couple of rinses with buffer TBS, samples were incubated with the suitable biotinylated or fluorochrome-conjugated secondary antibody diluted in 1% BSA in TBS for 45 min at room temperature. Samples incubated with fluorochrome-conjugated antibodies were washed in TBS and counterstained with DAPI for 10 min before imaging. Samples incubated with a biotinylated antibodies were washed in TBS and incubated with either the Avidin/Biotin Complex (ABC) solution conjugated to Alkaline Phosphatase (Vectastain ABC-AP Kit; Vector Laboratories; cat# AK-5000) or to Streptavidin-Horseadish Peroxidase (HRP) (Vectastain ABC-HRP Kit; Vector Laboratories; cat# PK-4000) for another 45 min at room temperature. After a couple of washing with TBS, samples were incubated with either the Vector Red Alkaline Phosphatase substrate solution (Vector Laboratories cat# SK-5100) or the Diaminobenzidine (DAB) substrate solution (Vector Laboratories cat# SK-4105) for 25 min and protected from light. Samples were washed for 1 min in TBS and counterstained with hematoxylin for 10 s. After washing hematoxylin excess with tap water, samples were mounted using Pertex mounting medium. Immunofluorescence imaging of polarized macrophages was performed as follows. Attached cells were fixed 1.5% PFA for 10 min and washed in PBS. Cells were then permeabilized with 0.1% Tween20 in PBS for 30 min and subsequently blocked for 30 min in 5% FBS in PBS. Cells were then incubated with PE anti-human CD80 or PE anti-human CD206 diluted in 2% FBS in PBS overnight at 4 °C. Afterwards, cells were washed in PBS and counterstained with DAPI for 10 min. Finally, cells were washed in PBS and imaged. Samples were acquired using Zeiss LSM 710 or Nikon AX/AXR confocal microscopes. Images quantification was performed using Image J/Fiji.

2.9. Glycosaminoglycans (GAG) quantification

Samples were digested overnight at 56 °C in 1 mL of proteinase K solution (Sigma Aldrich; cat# P2308) and GAG content was assessed using Glycosaminoglycan Assay Blyscan kit (Biocolor) according to manufacturer's instructions. GAG concentration was then normalized to the total amount of protein, which was calculated using PierceTM BCA Protein Assay Kit (ThermoFisher Scientific; cat# 23225) according to manufacturer's instructions.

2.10. HyC in vivo implantation

6-10 weeks-old female CD-1 Nude mice (Charles River; Crl:CD1-Foxn1nu) were used in this study. Animal experiments were approved by the Swiss Federal Veterinary Office (Permit 1797). Mice were provided with analgesia 1 h prior to the surgery by subcutaneous injection of Buprenorphin (0.1 mg/kg of body weight). During the surgery, mice were anesthetized with Isofluoran (2.5%) supplied on demand together with the oxygen (0.6 L/min). In preparation for the surgery, the back of the mouse was disinfected with 70% ethanol. Two midline incision of approximately 5 mm were made in the skin and 4 subcutaneous pockets (2 per incision) were generated in the back of each mouse using sterilized surgical material. HyC tissues were carefully introduced in the pockets with tweezers and finally the incisions were stapled. Mice were monitored after the surgery to discard adverse effects.

2.11. Microcomputed tomography (μCT)

Samples were explanted from the mice and directly fixed in 4% PFA overnight. μCT of *in vivo* remodeled tissues were performed using a SkyScan 1275 X-Ray Microtomograph (Bruker) with 70 kV as voltage and 260 μA as current. Transmission images were acquired for 360° with an incremental step size of 0.25°. Volumes were reconstructed using a modified Feldkamp algorithm (software supplied by manufacturer) at a voxel size of 10 μm. Thresholding, segmentation and 3D measurements were performed using the VG Studio Max software (Volume Graphics). An uniform threshold was defined to quantify the volume of mineralized/bone tissue (BV) relative to tissue total volume (TV). Trabecular (Tb) bone volume was estimated subtracting the cortical bone volume to the total volume.

2.12. Fluorescence-activated cell sorting (FACS) analysis

All explanted engineered tissues and native bones (femurs) were mechanically crushed and filtered through 40-μm strainer to obtain single-cell suspensions. For fully-remodeled and native BM tissues, samples were depleted of red blood cells by using a buffer lysis (EasySep RBC Lysis Buffer, StemCell Technologies cat#20120) for 10 min at 4 °C. The quantitative phenotype of the blood cells harvested from tissues was determined using a LSR II FORTESSA SORP (BD Biosciences) cell analyzer. Cells were labelled using the following fluorescent antibody conjugates with appropriate dilution (2–5 μg/ml) in PBS 2% FBS 0.5 M EDTA: APC-Cy7 Rat anti-mouse CD45 (BD Pharmigen; cat# 561037), APC Rat anti-CD11b (BD Pharmigen; cat# 553312), PE Rat anti-mouse Ly-6G (BD Pharmigen; cat# 551461), FITC Rat anti-mouse CD45R/B220 (BD Pharmigen; cat# 553087), PerCP-Cy5.5 Hamster anti-mouse CD3e (BD Pharmigen; cat# 561108), Biotin Mouse Lineage Depletion cocktail (BD Biosciences; cat# 51–9000794), PE Rat anti-mouse Ly-6A/E (BD Pharmigen; cat# 562059), PE-Cy7 anti-mouse CD117 (c-kit) (BioLegend; cat# 105814), APC anti-mouse CD150 (SLAM) (BioLegend; cat# 115909), PerCP/Cy5.5 anti-mouse CD48 (BioLegend; cat# 103421), BV711 anti-mouse Ly-6C (BioLegend; cat# 128037), PE anti-mouse F4/80 (BioLegend; cat# 123110), Alexa Fluor 647 anti-mouse CD206 (BioLegend; cat# 141712), PerCP/Cy5.5 anti-mouse/human CD11b (BioLegend; cat# 101228), BV711 anti-mouse CD115 (BioLegend; cat# 135515) and PE/Cy7 anti-mouse CD11c (BioLegend; cat#117318). Biotinylated antibodies were detected with APC-Cy7-conjugated streptavidin (BD Pharmigen; cat# 554063). Dead cells were excluded using DAPI (Sigma Aldrich; cat# 28710-90-3).

To analyze human macrophage immunophenotype after polarization, the following fluorescent antibodies were used: PE/Cy7 anti-human CD80 (BioLegend; cat# 305217), PerCP/Cy5.5 anti-human CD86 (BioLegend; cat# 374215), PE anti-human CD206 (BioLegend; cat# 321105) and APC/Cy7 anti-human 163 (BioLegend; cat# 333621).

2.13. Isolation of human monocytes

Human $CD14^+$ monocytes were isolated from human buffy coats collected from healthy donors at the Blutspendezentrum Basel as follows. Approximately 50–60 mL of buffy coat were diluted with 70 mL of PBS. Ficoll-Paque (VWR, cat# 17–1440) was added to the botton of Sepmate-50 tubes (StemCell Technologies; cat# 85450) for density gradient centrifugation. Diluted blood was slowly added on top of the Ficoll-Plaque and tubes were spun at 1400 rpm for 25 min with slow acceleration and no brakes. The cell mononuclear fraction was collected and placed in separated tubes. Two washing steps were performed with PBS 2% FBS 0.5 M EDTA before initiating the purification (positive selection) of human $CD14^+$ cells using CD14 MicroBeads (Milteny Biotec;

cat# 130-050-201) and LS columns (Miltenyi Biotec; cat# 130-042-401) according to manufacturer's instructions. Cell purity was checked by FACS staining for BV785 anti-human CD14 (BioLegend; cat# 301840), Alexa Fluor 488 mouse anti-human CD3 (BD Pharmigen; cat# 557694), PE/Cy7 anti-human CD19 (BioLegend; cat# 302215) and PE anti-human CD66b (BioLegend; cat# 305106).

2.14. In vitro human endothelial cells recruitment

Control or immunomodulatory HyC tissues were placed in 24-well plates. RFP^+ HUVECs were seeded in EGM-2 on 8 μm-pore size Transwell inserts (meshes) for these 24-wells plates (Greiner bio-one; PET membrane) at density of 10^4 cells per insert. After 1 week of culture, RFP^+ HUVECs recruited to the HyC tissues were measured by fluorescence imaging using a Nikon AX/AXR confocal microscope. Quantification was performed using Image J/Fiji.

2.15. In vitro human monocytes recruitment

$CD14^+$ cells isolated from human buffy coats as previously described were seeded in 1% Human Serum Albumine (HAS) RPMI on 8 μm-pore size Transwell inserts for 24-wells plates (Greiner bio-one; PET membrane) at density of $0.5*10^6$ cells per insert. Control or immunomodulatory HyC tissues were previously placed with RPMI medium in 24-well plates coated with 2% agarose. Plates were incubated at 37 °C for 16 h. After the incubation period, the HyC tissues were enzymatically-digested with collagenase II (320 u/mg), collagenase P (2.1 u/mg), 200 mM $CaCl_2$ in PBS for 30 min at 37 °C to retrieve the monocytes recruited to the tissue. $CD14^+CD66b^-$ cells (monocytes) were quantified by FACS.

2.16. In vitro human macrophage polarization

$CD14^+$ cells (isolated from human buffy coats as previously described) were seeded in 12-well plates at a density of $2*10^6$ cells per well with RPMI supplemented with 6.5 ng/mL Recombinant Human Macrophage Colony-Stimulating Factor (M-CSF) (Peprotech; cat# 300–25) and 6.5 ng/mL Recombinant Human Granulocyte-Macrophage Colony-Stimulating Factor (GM-CSF) (Peprotech; cat# 300–03), and cultured for 6 days to induce macrophage differentiation. After 6 days, old medium was replaced by fresh RPMI together with: (I) 20 ng/mL Interferon gamma (IFNγ; Sigma Aldrich; cat# SRP3058) and 20 ng/mL Lipopolysaccharide (LPS: Sigma Aldrich; cat# L2630) to induce control M1 macrophage polarization, (II) 20 ng/mL Recombinant human Interleukin 4 (IL4) (Peprotech; cat# 200–04) and 20 ng/mL Recombinant human Interleukin 13 (IL13) (Peprotech; cat# 200–13) to induce control M2 macrophage polarization, (III) crushed control HyC tissues and (IV) crushed IL1β-induced immunomodulatory HyC tissues. After 2 days of polarization, macrophages were then detached and processed for FACS and gene expression analyses.

2.17. In vitro human osteoclasts differentiation

$CD14^+$ cells (isolated from human buffy coats as previously described) were seeded in 12-well plates at a density of $0.5*10^6$ cells per well with αMEM supplemented with 20 ng/mL Recombinant Human M-CSF (Peprotech; cat# 300–25), and cultured for 6 days until reaching 80% confluency. Medium was replaced after 3 days. Osteoclast differentiation was induced by further culturing the cells in αMEM supplemented with 20 ng/mL Recombinant Human M-CSF (Peprotech; cat# 300–25) and 20 ng/mL Recombinant human soluble RANKL (Peprotech; cat# 310–01) for another 6 days (with medium change after 3 days). As experimental conditions, cells were also cultured with crushed control and IL1β-induced immunomodulatory HyC samples resuspended in medium with M-CSF and with/without RANKL. At final analysis, supernatants were collected for protein analysis and attached cells were processed for histological and gene expression analyses.

2.18. Statistical analysis and reproducibility

The compared groups were set similarly in all procedures and results were scored blindly. Data shown in figures are means ± standard deviation (SD); "n" values represent independent replicates and are indicated in the figure legends. One-Way ANOVA and Tukey comparison were used for multiple group comparisons, and unpaired two-tailed t tests for two-group comparisons. The data met the assumptions of the tests. Significant statistical differences between groups were indicated as: *$p < 0.05$; **$p < 0.01$; ***$p < 0.001$; ****$p < 0.0001$. Statistical analyses and graphics were carried out with GraphPad Prism 9 software.

3. Results

3.1. Engineering of a HyC matrix enriched in immunomodulatory factors through IL1β induction

We previously reported the potential of an immortalized cell line derived by human MSCs (MSOD-B) to generate *in vitro* HyC tissues [20]. Importantly, a critical requirement for MSOD-B cells to form HyC was their constitutive overexpression of BMP2. Following culture in collagen scaffolds in chondrogenic conditions for 3 weeks, the resulting tissues consisted in BMP2-enriched (about 40 ng per tissue) cartilaginous matrices which, even after devitalization, could fully remodel into bone and BM ossicles upon 6-weeks ectopic *in vivo* implantation [20].

In order to modulate the capacity of MSOD-B cells to produce immunomodulatory factors, we initially activated/primed MSOD-B cells by exposing them for 24 h to different immunoregulators such as IL1β, LPS, TNFα, polyinosinic:polycytidylic acid (poly (i:c)), IL4 and transforming growth factor β1 (TGFβ1), and measured the mRNA expression of different immune factors important for the early inflammatory phase. MSOD-B cells exhibited minimal expression levels of TNFα, IL10, IL4, IL13 and IFNγ (data not shown), while they expressed relevant levels of IL6, IL8, MCP1, IL1β, VEGF and, as expected, BMP2 (Supplementary Fig. 1). Some immunoregulators like TNFα and poly (i:c) triggered the upregulation of specific genes such as IL8, MCP1 and BMP2 (Supplementary Fig. 1B and C and 1F). TGFβ1 increased VEGF and BMP2 expression, but it did not activate the expression of pro-inflammatory cytokines (Supplementary Fig. 1F). In contrast, priming MSOD-B cells with IL1β was sufficient to upregulate the expression of *IL6*, *IL8*, *MCP1* and *IL1β* itself, both at the mRNA (Supplementary Figs. 1A–F) and protein level (Supplementary Figs. 1G–K). Since in wound healing these cytokines are known to play a crucial role in skewing early inflammation processes towards tissue vascularization, remodeling and regeneration [23,24], IL1β was selected as inducer for MSOD-B cells.

In order to generate HyC matrices enriched in these angiogenic and pro-inflammatory factors, MSOD-B cells were thus cultured for 3 weeks in collagen sponges in chondrogenic differentiation medium, as previously described [20], but with medium supplementation with IL1β (0.1 ng/mL) during the third week (Fig. 1A). In line with the results described above from 2D culture experiments, HyC matrices were enriched in IL6, IL8, MCP1 and VEGF, whereas BMP2 content remained similar to control HyC matrices without IL1β-induction (Fig. 2B–F). Interestingly, IL1β levels were undetectable in these matrices, suggesting that the inducer used to trigger the endogenous production of immunomodulatory factors by MSOD-B cells does not directly modulate the immune response.

Comparative histological and immunohistochemical analyses revealed a slight decrease in cartilage markers like glycosaminoglycans (GAG, labelled in pink in Safranin-O staining), collagen type II and collagen type X, but no differences were observed for the HyC marker MMP13 (Fig. 1G). GAG quantification and gene expression analysis confirmed these trends and showed a significant reduction only for *COL2A1* expression (Fig. 1H–K). These results demonstrate that IL1β can

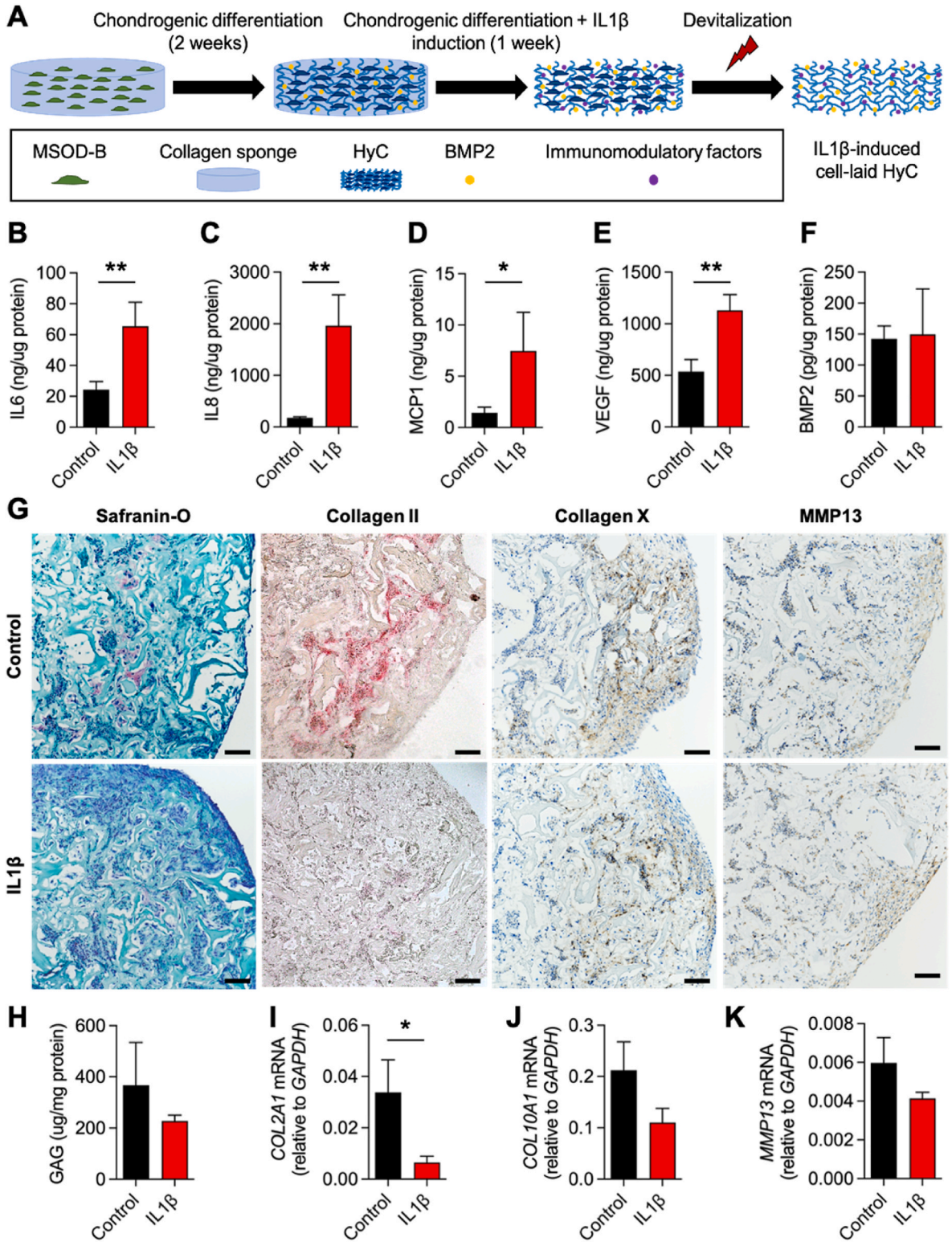

Fig. 1. Engineering of an immunomodulatory cell-laid HyC matrix using IL1β as inducer. (A) Scheme illustrating the protocol followed to generate a HyC matrix enriched in BMP2 (thanks to its overexpression by MSOD-B cells) and in immunomodulatory factors (thanks to MSOD-B cell induction with IL1β). (B–F) Protein concentration of (B) IL6, (C) IL8, (D) MCP1, (E) VEGF and (F) BMP2 in engineered control and IL1β-induced HyC matrices. (G) Safranin-O, Collagen type II, Collagen type X and MMP13 stainings in control and and IL1β-induced matrices. Scale bar, 100 μm. (H) Glycosamynoglycans (GAG) quantification in digested control and and IL1β-induced matrices. (I–K) Gene expression of (I) *COL2A1*, (J) *COL10A1* and (K) *MMP13* in control and and IL1β-induced matrices. (B–F), (H–K) Data are plotted as means ± SD; $n = 3$–12. $^{*}P < 0.05$, $^{**}P < 0.01$. Unpaired two-tailed *t*-test.

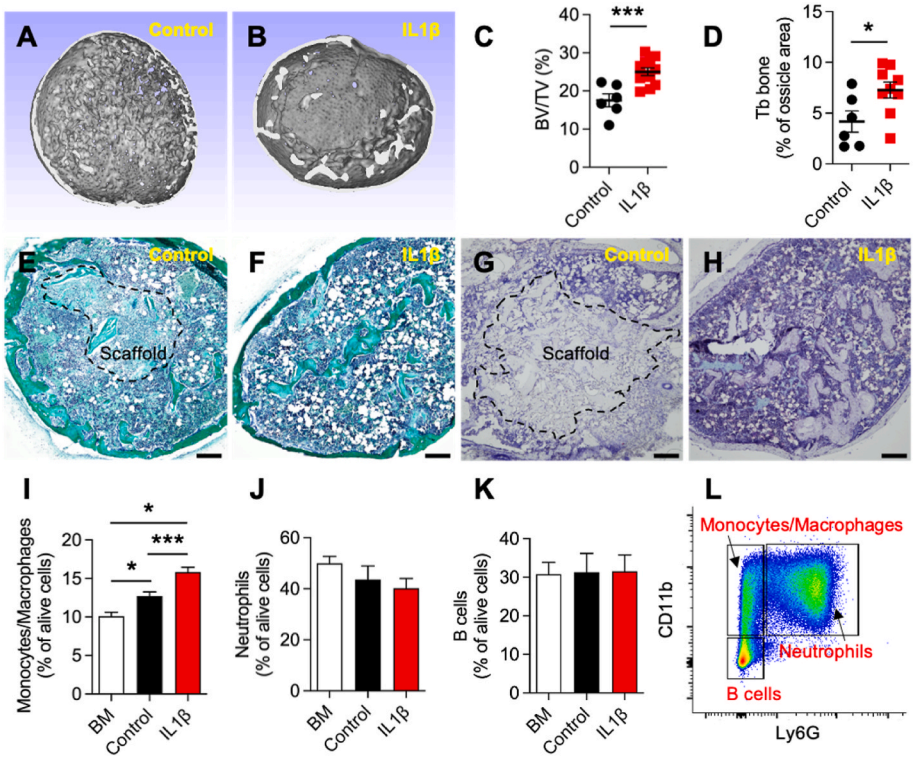

Fig. 2. IL1β-induced HyC matrix exhibits accelerated remodeling into endochondral bone. (A–B) Micro-computed tomography (μCT) 3D reconstructions showing mineralization in ossicles derived from control and IL1β-induced matrices after 3 weeks of *in vivo* remodeling. (C–D) Ratio Bone Volume (BV) to Total Volume (TV) and percentage of trabecular (Tb) bone in ossicles derived from control and IL1β-induced matrices after 3 weeks of *in vivo* remodeling. (E–F) Trichrome of Masson and (G–H) Hematoxylin-Eosin stainings in 10 μm-sections of ossicles derived from control and IL1β-induced matrices after 3 weeks of *in vivo* remodeling. Dashed lines delineate the areas occupied by the remaining parts of the scaffold. Scale bar, 20 μm. (I–K) Percentage of (I) $CD45^+CD11b^+Ly6G^-$ monocytes/macrophages, (J) $CD45^+CD11b^+Ly6G^+$ neutrophils and (K) $CD45^+B220^+$ B cells in the femoral BM, and in ossicles derived from control and IL1β-induced matrices after 3 weeks of *in vivo* remodeling. Percentages of these populations in femoral BM were used as additional control. (L) Representative FACS plot illustrating the gating for monocytes/macrophages, neutrophils and B cells in engineered tissues. (C-D; I–K) Data are plotted as means ± SD; $n = 3$–9. $^*P < 0.05$, $^{***}P < 0.001$. (C–D) Unpaired two-tailed *t*-test. (I–K) One-way ANOVA with Tukey's multiple comparison tests.

be used as inducer to enrich 3D HyC matrices in IL6, IL8, MCP1 and VEGF, with only slight reduction of the cartilaginous features.

3.2. IL1β-induced HyC matrix exhibits accelerated in vivo remodeling into endochondral bone

We next investigated the remodeling and endochondral bone formation capacity of IL1β-induced HyC matrices *in vivo*. Control (i.e., generated in the absence of IL1β) and IL1β-induced HyC tissues were subcutaneously implanted in mice for 3 weeks. μCT of the explanted samples showed abundant mineralized tissue in both cases (Fig. 2A and B); however, the amount of both total bone volume and trabecular bone was significantly increased in IL1β-induced HyC (Fig. 2C and D). Consistently, Masson's trichrome and hematoxylin/eosin stainings indicated that, as previously observed, control HyC tissues were only partially remodeled into bone/BM after 3 weeks, with cartilage/collagen scaffold remnants still present in the central part. In contrast, IL1β-induced HyC were already fully remodeled into ossicles with abundant trabecular bone and BM in the central part (Fig. 2E–H).

We then quantified the presence of progenitors and mature hematopoietic cells in these remodeled tissues after 3 weeks *in vivo* by FACS. Similar to the native BM tissue (femur) of CD-1 Nude mice, ossicles derived from engineered HyC tissues contained mostly neutrophils and B cells. No differences were observed between control and IL1β-induced matrices in these populations, whereas the percentage of monocytes/macrophages was enhanced in IL1β-induced HyC (Fig. 2I-L). The fractions of hematopoietic stem and progenitor cells (HSPCs) were unaffected and comparable to those measured in native BM tissues (Supplementary Fig. 2).

3.3. IL1β-induced cues promote vascular invasion, M2 macrophage polarization and osteoclast recruitment/differentiation after 1 week in vivo

In order to further investigate how IL1β-induced HyC could enhance *in vivo* bone formation upon ectopic implantation, we analyzed the implanted HyC after only 1 week *in vivo*.

After 1 week *in vivo* some $CD31^+$ vascular structures could be observed in the connective tissue surrounding the cartilaginous tissue (labelled by GFP-expressing MSOD-B cells), but only few of them invaded the matrix. In contrast, abundant vascularization was already found in the inner regions of IL1β-induced HyC tissues (Fig. 3A–C), suggesting that higher VEGF content enhanced vascular invasion. Increased vascular cells recruitment by IL1β-induced HyC was also confirmed *in vitro* coculturing RFP $^+$ HUVECs with HyC tissues in a Transwell system (Supplementary Figs. 3A–D). We next addressed if the increased vascularization had an impact on the recruitment of osteoprogenitor/osteoclastic cells. Immunostainings showed abundant $Osterix^+$ areas in HyC matrices (Fig. 3D–F), confirming the large density of osteoprogenitor cells in the remodeling tissues, but no differences were observed between tissues derived from control and IL1β-induced HyC. Instead, the density of $TRAP^+$ osteoclasts was three times higher in tissues derived from IL1β-induced HyC (Fig. 3G–I), consistently with the faster remodeling of the cartilage template. Immunophenotypic analysis of the hematopoietic cells harvested from the tissues revealed the dominance of myeloid cells at this stage. While classical monocytes and granulocytes, as well as the total fraction of $F4/80^+$ macrophages, were not differentially regulated (Fig. 3J-L and Supplementary Figs. 3E–F), the percentage of macrophages with a $CD206^+$ M2 phenotype was significantly higher in tissues derived from IL1β-induced HyC (Fig. 3L-M and Supplementary Figs. 3G–H). Finally, in agreement with TRAP staining results, the percentage of $CD11b^{low}cKit^+$ $CD115^+$ osteoclast precursors was doubled in tissues remodeled from IL1β-induced HyC matrices (Fig. 3N). Overall, these results suggest that the accelerated remodeling of tissues derived from IL1β-induced HyC is mediated by the activation of different myeloid cell populations, such as M2 macrophages and osteoclast precursors, as early as 1 week after *in vivo* implantation. Since these differences disappeared after 3 weeks *in vivo* (Supplementary Figs. 3I–K), we derive that the immunomodulating cytokines enriching the HyC elicit a short-term effect during the early phase of remodeling into endochondral bone.

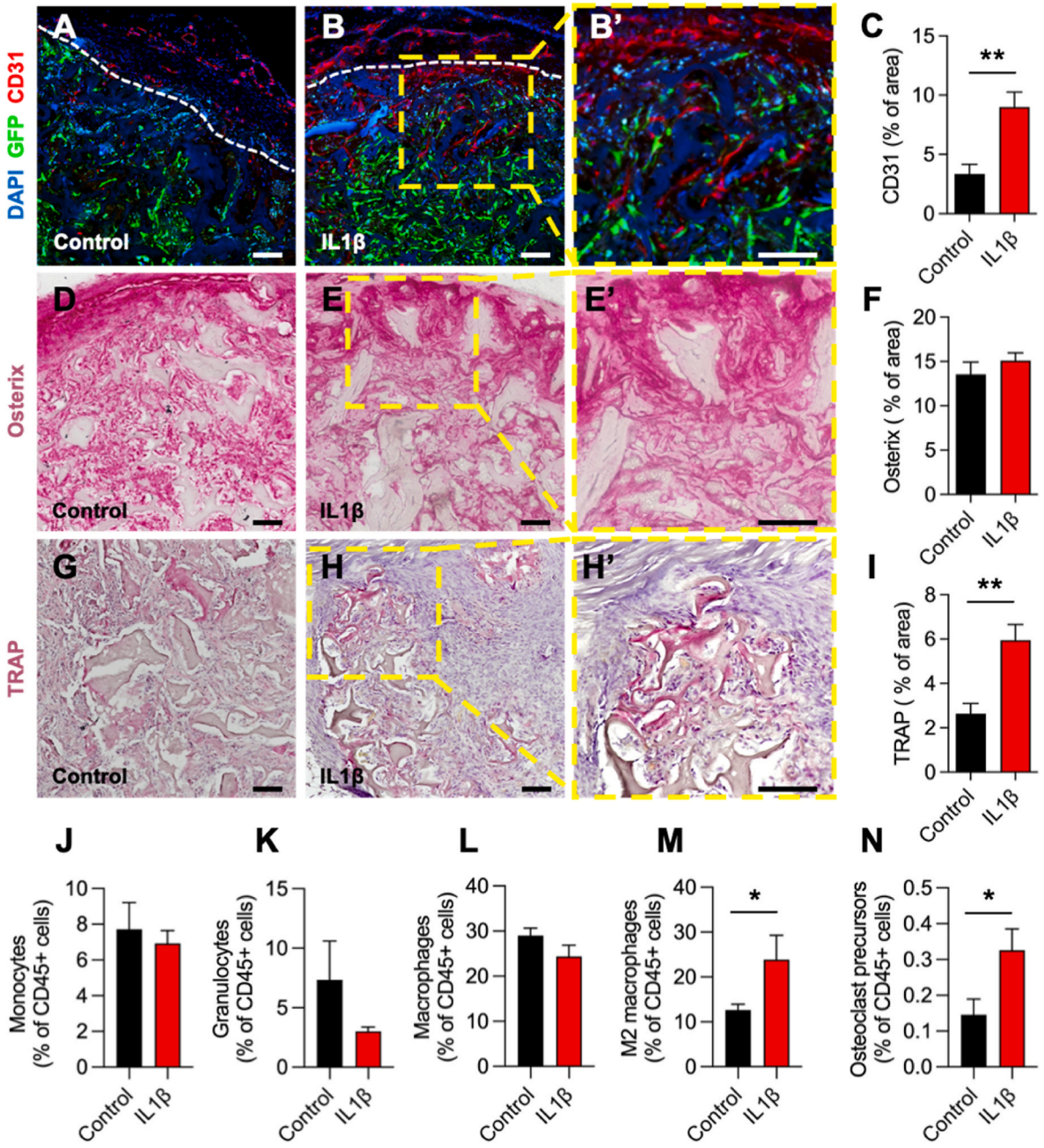

Fig. 3. IL1β-induced HyC promotes *in vivo* vascular recruitment, osteoclast activity and M2 macrophage polarization. (A–B) Immunofluorescent staining for CD31 (red) in 10 μm-sections of tissues derived from control and IL1β-induced matrices after 1 week of *in vivo* remodeling. MSOD-B-derived cells are labelled in green (GFP expression). Nuclei are labelled with DAPI (blue). The dashed lines delimitate the human cartilaginous tissue with MSOD-B cells from the surrounding mouse connective tissue. Scale bar, 100 μm. (C) Quantification of $CD31^+$ area in remodeled tissues after 1 week *in vivo*. (D–E) Immunostaining for Osterix in 10 μm-sections of tissues derived from control and IL1β-induced matrices after 1 week of *in vivo* remodeling. Scale bar, 100 μm. (F) Quantification of Osterix $^+$ area in remodeled tissues after 1 week *in vivo*. (G–H) Tartrate-resistant acid phosphatase (TRAP) staining in tissues derived from control and IL1β-induced matrices after 1 week of *in vivo* remodeling. Scale bar, 100 μm. (I) Quantification of TRAP $^+$ area in remodeled tissues after 1 week *in vivo*. (J–N) Percentage of (J) $CD11b^+Ly6G^-$ monocytes, (K) $CD11b^+Ly6G^+$ granulocytes, (L) $CD11b^+F4/80^+$ macrophages, (M) $CD11b^+F4/80^+CD206^+$ M2 macrophages and (N) $CD11b^{low}cKit^+CD115^+$ osteoclast precursors. (C, F, I, J-N) Data are plotted as means ± SD; $n = 5$. $^*P < 0.05$, $^{**}P < 0.01$. Unpaired two-tailed *t*-test.

3.4. IL1β-induced HyC upregulates IL6, TNFα and IL10 expression in human M2 macrophages

Based on the *in vivo* findings in mice, we then investigated whether IL1β-induction of HyC regulates also human macrophage differentiation and polarization, using an *in vitro* system. Briefly, $CD14^+$ myeloid cells were isolated from human peripheral blood and cultured with M-CSF and GM-CSF to induce macrophage differentiation for 6 days. After this period, macrophages were exposed to crushed control or IL1β-induced HyC matrices to induce polarization for 2 days. The combination of LPS and IFNγ were used as control to induce M1 macrophage polarization, whereas IL4 and IL13 were used to induce M2 macrophage polarization (Supplementary Figs. 4A–B). FACS analysis to detect CD80 and CD86 expression, as markers of M1 polarization, and CD206 and CD163, as markers of M2 polarization, revealed that both control and IL1β-induced HyC matrices induce a strong M2 polarization in this system (Fig. 4A–F). However, when we analyzed the gene expression profiles of macrophages we found that those exposed to IL1β-induced HyC matrices

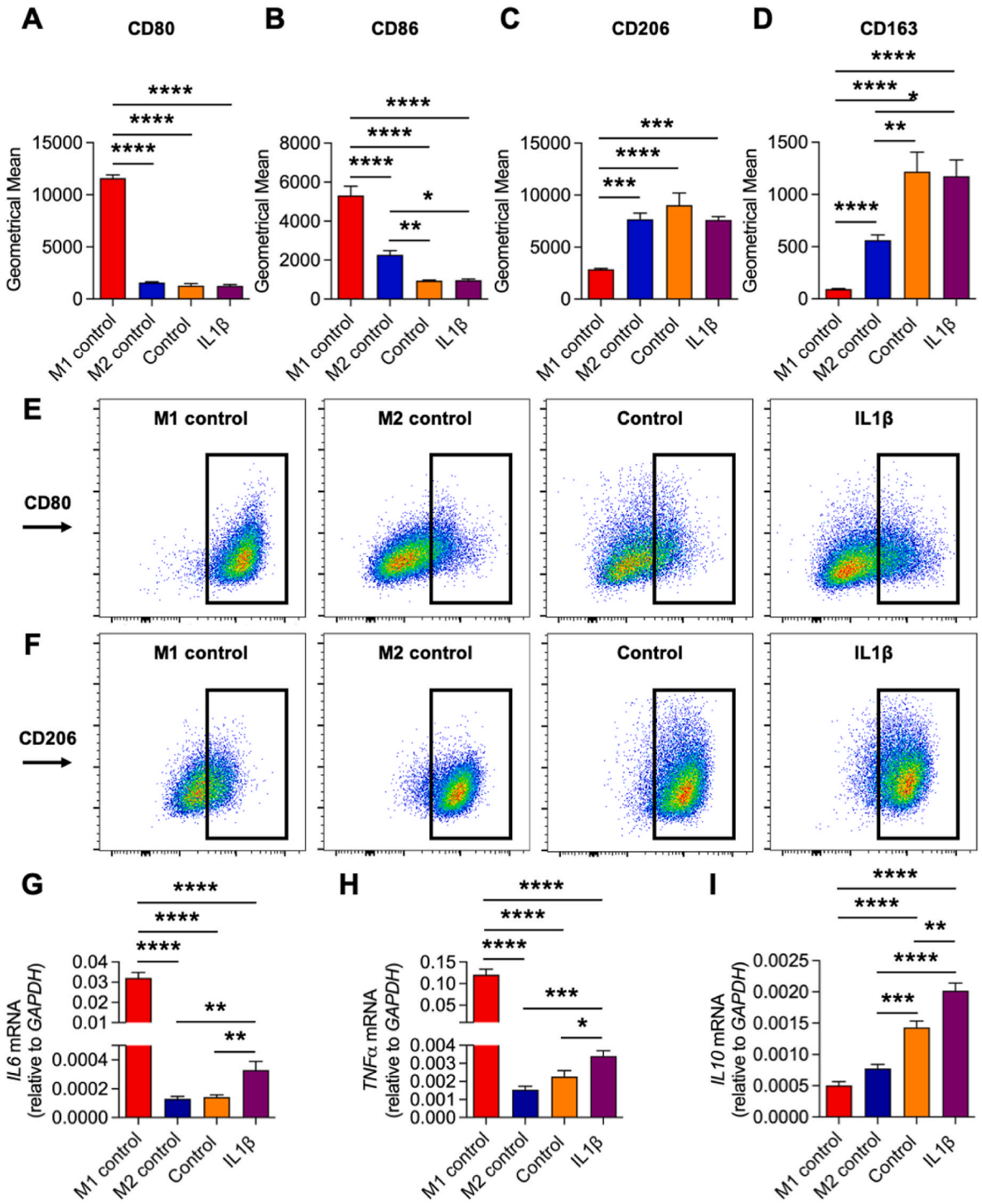

Fig. 4. IL1β-induced HyC upregulates *IL6*, *TNFα* and *IL10* expression *in vitro* in a model of human M2 macrophage polarization. (A–D) Geometrical mean of (A) CD80, (B) CD86, (C) CD206 and (D) CD163 protein surface expression of human macrophages exposed to M1 control differentiating signals, M2 control differentiating signals, crushed control and IL1β-induced HyC matrices. (E–F) Representative flow cytometry plots for (E) CD80 and (F) CD206 stainings in the different conditions. (G–I) Gene expression of (G) *IL6*, (H) *TNFα* and (I) *IL10* in human macrophages exposed to M1 control signals, M2 control signals, crushed control and IL1β-induced HyC matrices. (A-D, G-I) Data are plotted as means ± SD; $n = 6$. *$P < 0.05$, **$P < 0.01$, ***$P < 0.001$, ****$P < 0.0001$. One-way ANOVA with Tukey's multiple comparison tests.

expressed significantly higher levels of *IL6*, *TNFα* and *IL10* (Fig. 4G–I). These findings might indicate that early immunomodulatory signals provided by IL1β-induced HyC tissues are amplified by M2 polarized macrophages in a way that may predispose the environment towards regenerative events, as indicated by IL10 expression.

3.5. *IL1β-induced HyC enhances in vitro human osteoclast differentiation*

IL6 and TNFα are known as main players linking the immune and bone systems, and specifically to promote osteoclast differentiation and activation [25]. Indeed, our *in vivo* data indicated that IL1β-induced HyC, which is enriched in IL6 and TNFα, accelerates osteoclast-mediated

tissue remodeling (Fig. 3). We then investigated the possible effect of IL1β-induction of HyC on monocytes recruitment and osteoclast differentiation using human cells in two *in vitro* systems.

To assess monocytes recruitment, human peripheral blood-derived $CD14^+$ myeloid cells were cocultured with crushed control or IL1β-induced HyC matrices using a Transwell system. After 16 h, $CD14^+CD66b^-$ monocytes that migrated to the engineered HyC matrices were measured by FACS (Supplementary Fig. 4C). Control and IL1β-induced HyC matrices showed similar capacity to attract human monocytes (Supplementary Fig. 4D).

To assess differentiation of osteoclast precursors, human $CD14^+$ myeloid cells were first seeded and cultured for 6 days with M-CSF to induce macrophage differentiation, followed by another 6 days in coculture with crushed control or IL1β-induced HyC tissues, in presence or absence of RANKL, to induce osteoclast differentiation. Media supplemented with or without RANKL were used as positive and negative control, respectively (Supplementary Fig. 5A). As expected, the presence of RANKL was necessary to induce human macrophages generate large and multinucleated $TRAP^+$ osteoclasts (Supplementary Figs. 5B–E), as well as to increase levels of soluble TRAP (Supplementary Fig. 5F) and expression of MMP9 and CTSK (markers of osteoclast activity) (Supplementary Figs. 5G–H). Neither control nor IL1β-induced HyC matrices could induce osteoclast differentiation in the absence of RANKL; however, in those cultures supplemented with RANKL, IL1β-induced HyC samples lead to the formation of larger and more abundant $TRAP^+$ osteoclasts (Fig. 5A–H). Similarly, in the presence of RANKL, IL1β-induction of HyC was associated with higher levels of soluble TRAP (Fig. 5I) and of *MMP9* and *CTSK* expression (Fig. 5J and K), confirming the role of immunomodulatory signals trapped in the IL1β-induced HyC matrix in supporting human osteoclast differentiation.

4. Discussion

Here we engineered HyC matrix enriched in factors known to skew

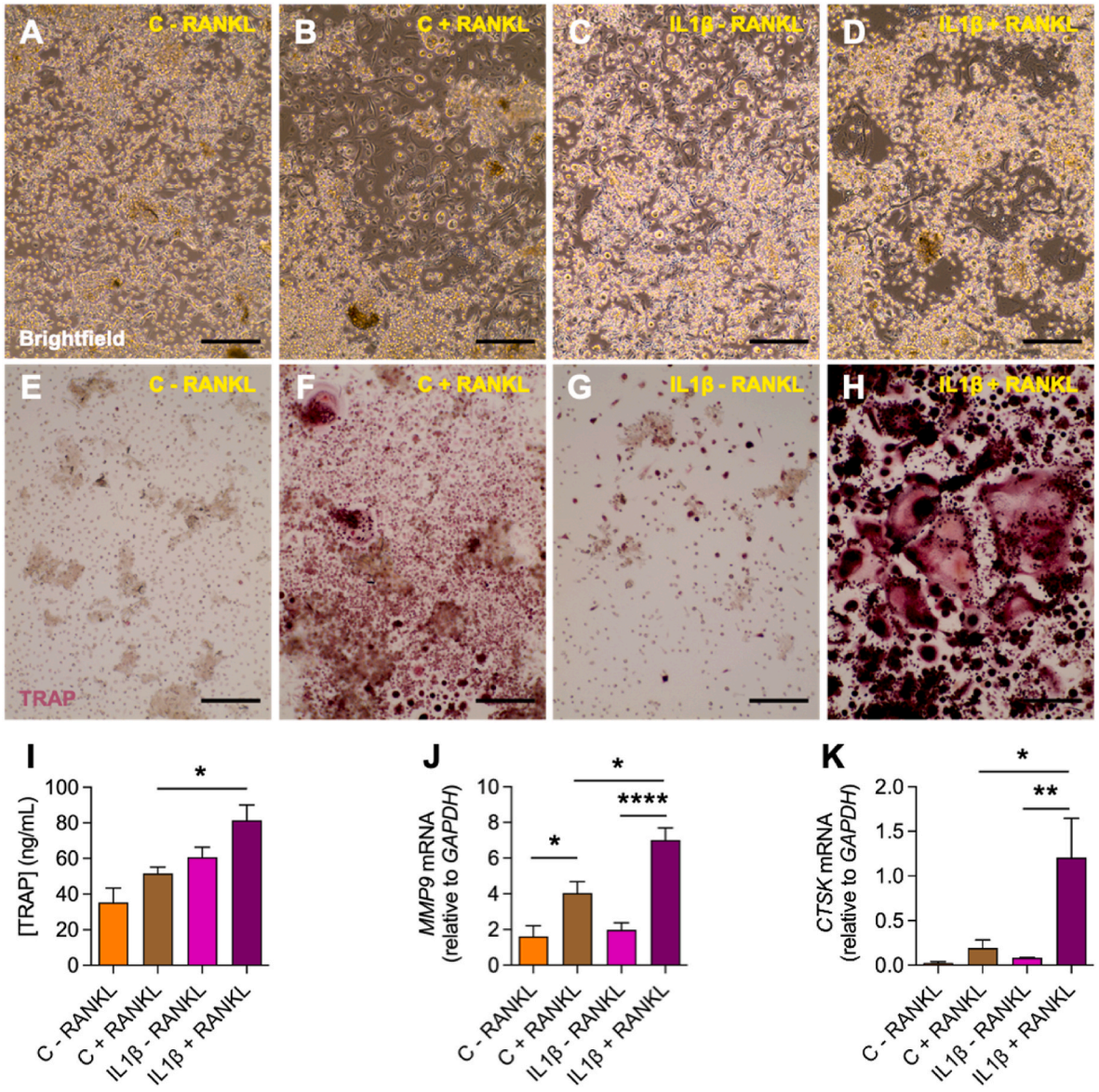

Fig. 5. IL1β-induced HyC enhances *in vitro* human osteoclast differentiation. (A–H) Brightfield images and TRAP staining in *in vitro* osteoclast cultures in presence of control ("C") and IL1β-induced ("IL1β") HyC matrices with (+) or without (−) RANKL. Scale bar, 500 μm. (I) TRAP quantification in osteoclast cultures in presence of control and IL1β-induced HyC matrices with/without RANKL. (J–K) Gene expression of (J) *MMP9 and* (K) *CTSK* in osteoclast cultures in presence of control and IL1β-induced HyC matrices with/without RANKL. (I–K) Data are plotted as means ± SD; $n = 6$. $^*P < 0.05$, $^{**}P < 0.01$, $^{****}P < 0.0001$. One-way ANOVA with Tukey's multiple comparison tests.

the early inflammatory phase in wound healing, in a way that conditioned immune cells towards remodeling and ultimately enhanced endochondral bone formation. Since such devitalized matrices could regulate macrophage polarization, accelerate angiogenesis and enhance myeloid cell differentiation to osteoclasts, we define them as *immunoinstructive materials*.

Bone fracture healing recapitulates most of the steps identified during developmental endochondral bone formation, which implies the formation of a transient cartilage template that will then remodel into bone upon the recruitment of vascular cells, osteoprogenitors and hematopoietic/immune cells. In order to recapitulate this process, we previously followed an engineering approach to generate *in vitro* a devitalized cartilaginous ECM enriched in osteoinductive cues such as BMP2 that, upon *in vivo* implantation, is able to reactivate these developmental processes leading to tissue remodeling into bone [16,20]. On the other hand, endochondral bone regeneration is greatly influenced by the innate immune system and controlled inflammatory signals were shown important to enhance the regenerative process in several bone tissue engineering approaches [24,26]. Only few studies attempted to modulate the early inflammatory phase to promote regenerative endochondral ossification, and most of them aimed at either suppressing M1 macrophages or directly promoting M2 polarization. However, cumulative evidences have demonstrated that ensuring pro-inflammatory and angiogenic cues at the early phase is as important as activating anti-inflammatory signals during the late anabolic endochondral phase [27].

Our findings illustrate how the combination of genetically-engineered cells producing BMP2 with IL1β induction to prime these cells allows the generation of an ECM including osteoinductive, angiogenic and pro-inflammatory signals, capable to activate endochondral ossification by coupling bone formation, vascularization and regulation of innate immunity. In contrast to previous studies based on living cells [14,16], our novel engineering approach does not only rely on the potential of IL1β to induce the secretion of angiogenic/pro-inflammatory factors during the *in vitro* chondrogenic differentiation of MSCs, but also on the capacity of the ECM to preserve these signals upon cell devitalization in order to elicit the effects *in vivo*. Native ECMs, including decellularized ones, also exhibit strong immunomodulatory properties [28,29], however they offer limited potential for customization in comparison to engineered ECMs. Other MSC derivatives such as extracellular vesicles are well-known to exhibit immunomodulatory properties in tissue repair and bone regeneration in particular [30,31]. In agreement with our work, a recent study has demonstrated that MSC preconditioning by another inflammatory factor (TNFα) allows the generation of immunomodulatory extracellular vesicles that influence macrophage polarization and enhance bone regeneration [32]. However, the immunomodulatory MSC secretome – in the absence of the osteoinductive factors embedded and delivered by the engineered ECM – is not sufficient to lead to *de novo* bone formation.

Whereas VEGF is the most potent angiogenic factor and its enrichment in our immunoinstructive HyC most likely enhanced cartilage remodeling into bone by facilitating vascular invasion [33], IL6, IL8 and MCP1 are potent pro-inflammatory factors that peak 24 h upon injury to recruit inflammatory cells such as monocytes and granulocytes. Some of these factors were also shown to later promote the recruitment of osteoprogenitor cells and contribute to the replacement of the cartilage matrix by activating proteases [34]. IL1β-induced engineered HyC matrices, enriched in these factors, skewed human macrophage immunophenotype towards M2 (*in vivo* results) and induced upregulation of IL6, TNFα and IL10 expression (*in vitro* results). However, further investigations should clarify the mechanisms underlying this processes. The fact that our *in vitro* results did not recapitulate the increase in the proportion of M2 macrophages observed *in vivo* might be explained by species-specific differences (mouse vs. human), or by the indirect contribution of other immune cells (i.e. monocytes and neutrophils) that are absent in the *in vitro* system. Our findings are consistent with the pivotal role for these innate immune cells in initiating bone regeneration after the early inflammatory phase [10]. In fact, IL10 is one of the main anti-inflammatory cytokines, might contribute to reinforce M2 macrophage polarization and trigger other regenerative signals [35,36], in addition to directly contributing to endochondral bone formation [37]. IL6 and TNFα are well-known to regulate both osteogenic and osteoclastic activity [17,38]. In this context, we detected a higher proportion of osteoclast precursors and TRAP-positive mature osteoclasts in implanted immunoinstructive HyC tissues after 1 week. This suggests that the more efficient remodeling of IL1β-induced HyC matrices into endochondral bone is mainly mediated by enhanced osteoclastic activity, leading to the resorption of the cartilage template and facilitating osteoprogenitors invasion. Further investigations should determine if this enhanced osteoclastic activity is directly caused or connected to IL6 and TNFα upregulation in M2 macrophages or vice versa. Although the impact of these engineered ECMs in the adaptive immunity is out of the scope of this study (CD1 nude mice lack T cells), we cannot neglect the potential effects of IL6, MCP1, RANTES, PGE2 and other inflammatory markers not addressed in this study on B and T cells [39].

In conclusion, here we present a novel category of immunoinstructive off-the-shelf materials and demonstrate their potent osteoinductive properties by recapitulation of endochondral ossification. Further investigations should determine if this enhanced osteoinductivity leads to a more efficient bone healing in an in-situ, orthotopic implantation model. More broadly, we propose a strategy to engineer ECMs encoding molecular instructions capable to skew early inflammatory processes *in vivo* towards regeneration. This approach may find application to target defined requirements of tissue healing, thanks to the potential for customization which is enabled by (i) the cell lines used and (ii) their specific immune-priming and conditioning.

Ethics approval

Animal experiments were approved by the Swiss Federal Veterinary Office (Permit 1797). Human $CD14^+$ cells were isolated from human buffy coats collected from healthy donors at the Blutspendezentrum Basel. All experiments were compliant with European Union recommendations.

CRediT authorship contribution statement

Andrés García-García: Conceptualization, Methodology, Formal analysis, Investigation, Data curation, Writing – original draft, Writing – review & editing, Visualization, Project administration. **Sébastien Pigeot:** Methodology, Validation, Investigation. **Ivan Martin:** Conceptualization, Writing – original draft, Writing – review & editing, Supervision, Project administration, Funding acquisition.

Declaration of conflicting interest

The author(s) declared no potential conflicts of interest with respect to the research, authorship, and/or publication of this article.

Acknowledgments

We thank the Department of Biomedicine core facilities for assistance and support. This work was supported by the Swiss National Science Foundation Div 3 (Grant 31003A-179259 to I.M.) and the National Centre of Competence in Research (NCCR) Molecular Systems Engineering (Grant 51NF40-141825 to I.M.).

Appendix A. Supplementary data

Supplementary data to this article can be found online at https://doi.org/10.1016/j.bioactmat.2022.12.017.

References

[1] J. Rho, M. Takami, Y. Choi, Osteoimmunology: interactions of the immune and skeletal systems, Mol. Cell 17 (1) (2004) 1–9.
[2] H. Takayanagi, Osteoimmunology: shared mechanisms and crosstalk between the immune and bone systems, Nat. Rev. Immunol. 7 (4) (2007) 292–304.
[3] H.M. Kronenberg, Developmental regulation of the growth plate, Nature 423 (6937) (2003) 332–336.
[4] T.A. Einhorn, L.C. Gerstenfeld, Fracture healing: mechanisms and interventions, Nat. Rev. Rheumatol. 11 (1) (2015) 45–54.
[5] T. Ono, H. Takayanagi, Osteoimmunology in bone fracture healing, Curr. Osteoporos. Rep. 15 (4) (2017) 367–375.
[6] G.S. Baht, L. Vi, B.A. Alman, The role of the immune cells in fracture healing, Curr. Osteoporos. Rep. 16 (2) (2018) 138–145.
[7] Y. Niu, et al., Modulating macrophage activities to promote endogenous bone regeneration: biological mechanisms and engineering approaches, Bioact. Mater. 6 (1) (2021) 244–261.
[8] A. Garcia-Garcia, I. Martin, Extracellular matrices to modulate the innate immune response and enhance bone healing, Front. Immunol. 10 (2019) 2256.
[9] L.J. Raggatt, et al., Fracture healing via periosteal callus formation requires macrophages for both initiation and progression of early endochondral ossification, Am. J. Pathol. 184 (12) (2014) 3192–3204.
[10] C. Schlundt, et al., Macrophages in bone fracture healing: their essential role in endochondral ossification, Bone 106 (2018) 78–89.
[11] J.K. Chan, et al., Low-dose TNF augments fracture healing in normal and osteoporotic bone by up-regulating the innate immune response, EMBO Mol. Med. 7 (5) (2015) 547–561.
[12] L.C. Gerstenfeld, et al., Impaired intramembranous bone formation during bone repair in the absence of tumor necrosis factor-alpha signaling, Cells Tissues Organs 169 (3) (2001) 285–294.
[13] J. Lange, et al., Action of IL-1beta during fracture healing, J. Orthop. Res. 28 (6) (2010) 778–784.
[14] M. Mumme, et al., Interleukin-1beta modulates endochondral ossification by human adult bone marrow stromal cells, Eur. Cell. Mater. 24 (2012) 224–236.
[15] P. Guihard, et al., Induction of osteogenesis in mesenchymal stem cells by activated monocytes/macrophages depends on oncostatin M signaling, Stem Cell. 30 (4) (2012) 762–772.
[16] C. Scotti, et al., Engineering of a functional bone organ through endochondral ossification, Proc. Natl. Acad. Sci. U. S. A. 110 (10) (2013) 3997–4002.
[17] X. Yang, et al., Callus mineralization and maturation are delayed during fracture healing in interleukin-6 knockout mice, Bone 41 (6) (2007) 928–936.
[18] M. Croes, et al., Proinflammatory mediators enhance the osteogenesis of human mesenchymal stem cells after lineage commitment, PLoS One 10 (7) (2015), e0132781.
[19] N. Su, C. Villicana, F. Yang, Immunomodulatory strategies for bone regeneration: a review from the perspective of disease types, Biomaterials 286 (2022) 121604.
[20] S. Pigeot, et al., Manufacturing of human tissues as off-the-Shelf grafts programmed to induce regeneration, Adv. Mater. 33 (43) (2021), e2103737.
[21] Y.M. Lee, et al., IL-1 plays an important role in the bone metabolism under physiological conditions, Int. Immunol. 22 (10) (2010) 805–816.
[22] P. Bourgine, et al., Combination of immortalization and inducible death strategies to generate a human mesenchymal stromal cell line with controlled survival, Stem Cell Res. 12 (2) (2014) 584–598.
[23] P. Bao, et al., The role of vascular endothelial growth factor in wound healing, J. Surg. Res. 153 (2) (2009) 347–358.
[24] P.M. Mountziaris, A.G. Mikos, Modulation of the inflammatory response for enhanced bone tissue regeneration, Tissue Eng. B Rev. 14 (2) (2008) 179–186.
[25] T. Wang, C. He, TNF-Alpha and IL-6: the Link between Immune and bone system, Curr. Drug Targets 21 (3) (2020) 213–227.
[26] M. Maruyama, et al., Modulation of the inflammatory response and bone healing, Front. Endocrinol. 11 (2020) 386. Lausanne.
[27] S.K. Chow, et al., Modulating macrophage polarization for the enhancement of fracture healing, a systematic review, J Orthop Translat 36 (2022) 83–90.
[28] J.L. Dziki, et al., Extracellular matrix bioscaffolds as immunomodulatory Biomaterials<sup/>, Tissue Eng. 23 (19–20) (2017) 1152–1159.
[29] X. Zhang, et al., Decellularized extracellular matrix scaffolds: recent trends and emerging strategies in tissue engineering, Bioact. Mater. 10 (2022) 15–31.
[30] C. Marar, B. Starich, D. Wirtz, Extracellular vesicles in immunomodulation and tumor progression, Nat. Immunol. 22 (5) (2021) 560–570.
[31] P.K. L, et al., The mesenchymal stem cell secretome: a new paradigm towards cell-free therapeutic mode in regenerative medicine, Cytokine Growth Factor Rev. 46 (2019) 1–9.
[32] M. Kang, et al., Extracellular vesicles from TNFalpha preconditioned MSCs: effects on immunomodulation and bone regeneration, Front. Immunol. 13 (2022) 878194.
[33] K. Hu, B.R. Olsen, Vascular endothelial growth factor control mechanisms in skeletal growth and repair, Dev. Dynam. 246 (4) (2017) 227–234.
[34] R. Dimitriou, E. Tsiridis, P.V. Giannoudis, Current concepts of molecular aspects of bone healing, Injury 36 (12) (2005) 1392–1404.
[35] K.N. Couper, D.G. Blount, E.M. Riley, IL-10: the master regulator of immunity to infection, J. Immunol. 180 (9) (2008) 5771–5777.
[36] N. Makita, et al., IL-10 enhances the phenotype of M2 macrophages induced by IL-4 and confers the ability to increase eosinophil migration, Int. Immunol. 27 (3) (2015) 131–141.
[37] Y.K. Jung, et al., Role of interleukin-10 in endochondral bone formation in mice: anabolic effect via the bone morphogenetic protein/Smad pathway, Arthritis Rheum. 65 (12) (2013) 3153–3164.
[38] R. Balga, et al., Tumor necrosis factor-alpha: alternative role as an inhibitor of osteoclast formation in vitro, Bone 39 (2) (2006) 325–335.
[39] D. Kyurkchiev, et al., Secretion of immunoregulatory cytokines by mesenchymal stem cells, World J. Stem Cell. 6 (5) (2014) 552–570.